Textile Research Journal

http://trj.sagepub.com

Fragmentation in a Model Two-Component Fibrous Structure

Thomas A. Godfrey and Suzanne E. Bosselman

Textile Research Journal 2006; 76; 883
DOI: 10.1177/0040517506057444

The online version of this article can be found at:
http://trj.sagepub.com/cgi/content/abstract/76/12/883

Published by:
SAGE Publications
http://www.sagepublications.com

Additional services and information for *Textile Research Journal* can be found at:

Email Alerts: http://trj.sagepub.com/cgi/alerts

Subscriptions: http://trj.sagepub.com/subscriptions

Reprints: http://www.sagepub.com/journalsReprints.nav

Permissions: http://www.sagepub.com/journalsPermissions.nav

Downloaded from http://trj.sagepub.com at US ARMY SOLDIER BIOCHEM COMM on May 8, 2008
© 2006 SAGE Publications. All rights reserved. Not for commercial use or unauthorized distribution.

Textile Research Journal | Article

Fragmentation in a Model Two-Component Fibrous Structure

Thomas A. Godfrey[1] and Suzanne E. Bosselman
Natick Soldier Center, U.S. Army Research, Development & Engineering Command, Natick, Massachusetts 01760-5020, U.S.A.

Abstract A simple micromechanical model for the deformation of an isolated fiber fragment embedded within a bundle of continuous filaments is used to study progressive fragmentation of the low elongation-to-break (LE) fiber component during extension of a model two-component fibrous structure. The model structure, representing a blended yarn or cord, is realized in experimental specimens by helically wrapping a number of high elongation-to-break (HE) components around a straight central LE component; polyester sewing thread and cotton sewing thread are used is this work as the HE and LE components, respectively. The concept of a characteristic fragment length, involving the failure statistics of a fragment as influenced by the interaction forces between the fragment and the surrounding fibrous medium, is used to interpret the fragmentation experiments and calibrate a dimensionless parameter in the micromechanical model. The calibrated model is shown to provide insight into force interactions between the fragment and the surrounding structure. Bounds are established on the force interaction behavior associated with possible variations in the value of a constitutive parameter.

Key words fragmentation, shear forces, fiber strains, friction, fibrous assemblies

In fibrous composite materials, many studies have shown the significant influence of the fiber/matrix interfacial zone on overall mechanical properties of the composite, representative works include Achenbach and Zhu [1] and Chawla [2]. The interactions occurring at the fiber-to-fiber interface in assemblies of dry fibers are similarly of critical importance to the mechanical behavior of yarns, cords, and fabrics. In comparison with fibrous composites, little work has been done to investigate the influence of interfacial forces and behavior in dry fibrous (textile) structures.

In yarns and cords, fiber-to-fiber interfaces occur between nominally parallel fibers packed in an array (the local microstructure of the yarn) and laterally compressed by internal forces developed in the yarn during extension due to twist. As the yarn extends, the fiber-to-fiber interface acts to pass compressive and shear forces between

Textile Research Journal Vol 76(12): 883–895 DOI: 10.1177/0040517506057444 www.trj.sagepub.com © 2006 SAGE Publications

Downloaded from http://trj.sagepub.com at US ARMY SOLDIER BIOCHEM COMM on May 8, 2008
© 2006 SAGE Publications. All rights reserved. Not for commercial use or unauthorized distribution.

abutting fibers. In theoretical analyses of the extension of twisted continuous filament yarns, it has been common practice to neglect shearing forces parallel to the local filament direction – the filaments are assumed to slip without friction relative to their neighbors as the twisted structure extends. Such analyses have been quite successful in predicting yarn load-extension behavior; the reader is referred to Hearle [3] for a detailed development and review of the literature. In contrast, for yarns made from staple fibers, shearing forces arising near the ends of the fiber are essential – the yarn simply slips apart if the shearing forces are inadequate [4, pp. 40–43]. Inter-fiber shear forces become important in continuous filament yarns during the failure process, since they occur near fiber breaks and control how loads are passed from one fiber to the next, influencing the progression of fiber breakage during yarn extension. Shear is transferred through interfacial deformation and contact over regions of relative slip at the interface, and over regions where the interface does not slip. The central aim of the present paper is to introduce a semi-empirical approach to quantify the shear forces at the fiber-to-fiber interface in a fibrous structure through progressive fragmentation experiments.

Knowledge of inter-fiber shearing forces is especially important to the development of advanced hybrid or blended yarns, where the interactions between different fiber types can be exploited to achieve high strength in combination with high elongation-to-break. In such yarns, stiff low elongation-to-break (LE) fibers are intermingled among more compliant high elongation-to-break (HE) fibers. During extension, the LE fibers undergo successive fragmentation, but with proper interaction with surrounding HE fibers, continue to reinforce and carry load as part of the yarn structure. Godfrey and Rossettos [5] developed a micromechanical model for the interactions between an isolated LE fiber fragment embedded in a bundle of continuous HE filaments. The fiber bundle is modeled as a square-stacked array of parallel rods with appropriate surface tractions corresponding to regions of slip and elastic interaction at abutting fiber surfaces. Key results from the model include degree of reinforcement provided by the LE fragment (i.e., the portion of the total fiber bundle load that may be attributed to the fragment), and the strain profiles in the LE fragment and surrounding HE filaments. Results depended strongly on the extent of the slipping region along the interface, which involved elastic properties of the fibers and interface as well as the frictional slip shear traction along the slipping region. For the model to be useful in the design of advanced hybrid yarns, such information needs to be obtained through a semi-empirical approach. In the present work, we use such an approach to gain insight into the frictional shear traction, q_s, as it occurs during fragmentation in a model system.

In this paper, adopting the basic modeling approach taken in [5], we derive a simplified micro-mechanical model for the deformation of an isolated LE fiber fragment embedded within a bundle of continuous HE filaments. We develop the cumulative distribution function for failure (subsequent fragmentation) of a LE fragment at a prescribed nominal strain in the bundle, where the strain profile along the fragment is given by the micro-mechanical model. The fragment failure distribution is used to interpret progressive fragmentation in a special two-component strand consisting of a central straight LE component helically wrapped by 24 HE components. Strand specimens are extended to 8, 10, 12, 15, and 18% nominal strain, and the lengths and condition of the LE fragments are cataloged and used to estimate a 'characteristic fragment length,' a fragment length for which the cumulative probability of failure at a given strain level is 50%. The experimental characteristic lengths are used to calibrate a model parameter, the nondimensional slip region extent, in the analytical fragment failure distribution, thereby providing the frictional shear traction and extent of slip along the interface. The frictional shear traction, q_s, determined from the fragmentation data, is found to be in reasonable agreement with a prediction of the behavior of q_s with increasing strand strain based on Amontons' Law and the mechanics of deformation of the helically wrapped strand structure.

Micromechanical Model

Development

Consider an LE fiber fragment, length $2l$, embedded in a bundle or mass of filaments. In general, the surrounding filaments may consist of both HE and LE fibers, which we regard in this simplest possible model as a homogeneous medium. The fragment and its immediate surroundings represent the local microstructure at some point within a yarn or cord. As discussed previously, axial extension of yarns and cords induces transverse compressive forces. Therefore, it is assumed that the global deformation of the yarn when extended leads to extension of the bundle along the fragment axial direction combined with compression acting in the transverse plane.

The fragment lies along the x-coordinate axis, with the origin placed at the fragment tip (Figure 1). To develop the simplest possible model, we ignore the individual response of discrete filaments surrounding the fragment. Therefore, the x-direction strain everywhere in the fibrous bundle is taken to be the average or applied strain ε. The fragment is assumed to behave as a linear elastic rod loaded by surface shear tractions due to interaction with the surrounding fibers. Introduce $u(x)$ as the displacement of points on the fragment relative to a uniformly strained reference with strain ε. The total displacement of points on the fragment, $u^*(x)$, may be expressed as $u^*(x) = u(x) + \varepsilon x$. Force equilibrium for the fragment is written as

Downloaded from http://trj.sagepub.com at US ARMY SOLDIER BIOCHEM COMM on May 8, 2008
© 2006 SAGE Publications. All rights reserved. Not for commercial use or unauthorized distribution.

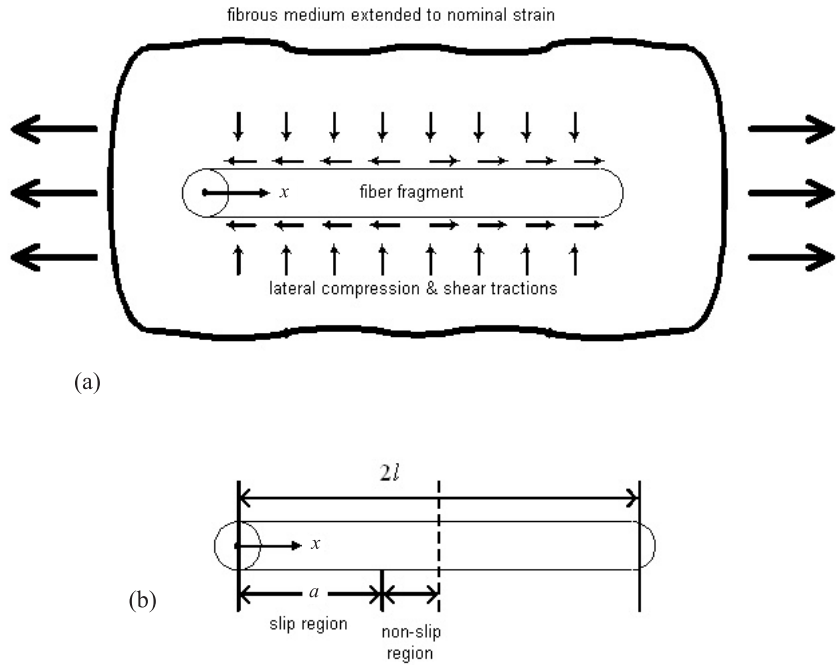

Figure 1 (a) Fragment embedded in HE medium with system of forces. (b) Slip region and non-slip region geometry.

$$EA\frac{d^2u}{dx^2} + q(x) = 0 \tag{1}$$

where EA is the extensional stiffness of the fragment (dimensions of force) and $q(x)$ represents the total shear force per length on the fragment at position x.

The fragment's interaction with the medium is symmetric with respect to the fragment midpoint, so we need only deal with the half fragment lying in $0 \le x \le l$. Slip between the fragment and the surrounding medium is assumed to occur in a region near the fragment tip, $0 \le x \le a$, where $a < l$ (Figure 1b). In the slip region, $q(x)$ takes on the constant value $-q_s$, which will depend on particulars of the structure and the applied strain (Figure 2). In the region where slip is not occurring, $a < x \le l$, we assume $q(x)$ is proportional to the difference between the total displacement of the surrounding medium and that of the fragment. Noting the surrounding medium's total displacement is $u_m^* \cong \varepsilon x$, it can be seen that $q(x)$ may be written as $q(x) = -ku$, where k is interpreted as an elastic constant, dimensions of force/length^2, representing shearing of the interface between the fragment and the abutting fibrous material.

Non-dimensional position coordinate, ξ, and displacement variable, U, are introduced

$$x = \sqrt{EA/k}\,\xi, \quad u = \varepsilon\sqrt{EA/k}\,U. \tag{2a, 2b}$$

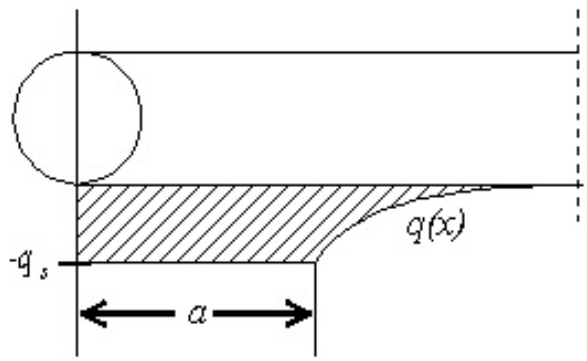

Figure 2 Shear force per length along fragment.

Equation (1) is written in non-dimensional form, using equations (2a) and (2b), where the appropriate expression for $q(x)$ in the slipping and non-slipping region, has been taken, as

$$\text{slip region:} \quad \frac{d^2U}{d\xi^2} - Q = 0, \quad 0 < \xi \le \alpha; \tag{3}$$

$$\text{non-slip region:} \quad \frac{d^2U}{d\xi^2} - U = 0, \quad \alpha < \xi \le L; \tag{4}$$

Downloaded from http://trj.sagepub.com at US ARMY SOLDIER BIOCHEM COMM on May 8, 2008
© 2006 SAGE Publications. All rights reserved. Not for commercial use or unauthorized distribution.

where $Q = \frac{q_s}{\varepsilon\sqrt{kEA}}$, and a dimensionless fragment half length and slip region extent are defined, using equation (2a), as $(l, a) = \sqrt{EA/k}(L, \alpha)$.

Boundary conditions consist of a stress-free condition at the fragment tip, $[\mathrm{d}u^*/\mathrm{d}x]_{x=0} = 0$, and a symmetry condition at the fragment midpoint, $u(l) = 0$. In the dimensionless variables, the midpoint boundary condition becomes $U(L) = 0$. Using the definition of the displacement reference, i.e. $u^*(x) = u(x) + \varepsilon x$, it can easily be shown that the stress-free boundary condition becomes $[\mathrm{d}U/\mathrm{d}\xi]_{\xi=0} = -1$.

In the following, we denote the slip and non-slip regions as regions I and II, respectively, and indicate the displacements in each region through Roman numeral subscripts. In region I, integrating equation (3) once and applying the stress-free condition, we obtain

$$\frac{\mathrm{d}U_{\mathrm{I}}}{\mathrm{d}\xi} = Q\xi - 1 \tag{5}$$

Integrating once more

$$U_{\mathrm{I}} = \frac{Q\xi^2}{2} - \xi + C \tag{6}$$

In region II, the solution for equation (4) is written as $U_{\mathrm{II}} = D\mathrm{e}^{-\xi} + F\mathrm{e}^{+\xi}$. The integration constant F may be eliminated using the midpoint symmetry condition to obtain

$$U_{\mathrm{II}} = D(\mathrm{e}^{-\xi} - \mathrm{e}^{\xi-2L}) \tag{7}$$

Displacement, strain, and the shear force per length $q(x)$ are continuous across the boundary between the slipping and non-slipping regions. To develop the shear force continuity condition, we write $q(x)|_{x\to a} = -q_s = -EA\left.\frac{\mathrm{d}^2U_{\mathrm{II}}}{\mathrm{d}x^2}\right|_{x\to a}$, where we have made use of equation (1). The three continuity conditions, representing displacement, strain, and shear force/length continuity, respectively, are written in nondimensional form as

$$U_{\mathrm{I}}(\alpha) = U_{\mathrm{II}}(\alpha), \quad \left.\frac{\mathrm{d}U_{\mathrm{I}}}{\mathrm{d}\xi}\right|_{\xi=\alpha} = \left.\frac{\mathrm{d}U_{\mathrm{II}}}{\mathrm{d}\xi}\right|_{\xi=\alpha}, \tag{8a, 8b}$$

$$\left.\frac{\mathrm{d}^2U_{\mathrm{II}}}{\mathrm{d}\xi^2}\right|_{\xi=\alpha} = Q \tag{8c}$$

where equation (8c) may be expressed conveniently as $U_{\mathrm{II}}(\alpha) = Q$, using equation (4).

The integration constants C and D, and the parameter Q, may be solved for in terms of the slip region extent, α, and fragment length, L, through application of the three continuity conditions. The parameter Q is found to be

$$Q = \frac{\mathrm{e}^{-\alpha} - \mathrm{e}^{\alpha-2L}}{(1+\alpha)\mathrm{e}^{-\alpha} + (1-\alpha)\mathrm{e}^{\alpha-2L}}. \tag{9}$$

The displacements become

$$U_{\mathrm{I}} = \frac{1}{2}Q(\xi^2 - \alpha^2 + 2) - \xi + \alpha, \tag{10}$$

in the slip region, $0 \le \xi \le \alpha$, and

$$U_{\mathrm{II}} = \frac{\mathrm{e}^{-\xi} - \mathrm{e}^{\xi-2L}}{(1+\alpha)\mathrm{e}^{-\alpha} + (1-\alpha)\mathrm{e}^{\alpha-2L}}, \tag{11}$$

in the non-slip region, $\alpha \le \xi \le L$.

Our main interest is in the fragment strain, $\varepsilon_{\mathrm{frag}}(\xi)$, for given values of the applied strain, ε, fragment length and slip region extent. Note that fragment strain is $\mathrm{d}u^*/\mathrm{d}x$ where u^* is the total displacement and $u^* = u + \varepsilon x$. Therefore, fragment strain may be written as $\varepsilon_{\mathrm{frag}} = \mathrm{d}u/\mathrm{d}x + \varepsilon$. Non-dimensionalizing, using equations (2a) and (2b), we obtain

$$\varepsilon_{\mathrm{frag}} = \left(\frac{\mathrm{d}U}{\mathrm{d}\xi} + 1\right)\varepsilon \tag{12}$$

Using equation (12) in combination with equation (5) for region I, and the first derivative of equation (11) for region II, we write the fragment strains as

$$\varepsilon_{\mathrm{frag\,I}} = Q\xi\varepsilon, \quad 0 \le \xi \le \alpha; \tag{13}$$

and

$$\varepsilon_{\mathrm{frag\,II}} = \left\{1 - \frac{\mathrm{e}^{-\xi} + \mathrm{e}^{\xi-2L}}{(1+\alpha)\mathrm{e}^{-\alpha} + (1-\alpha)\mathrm{e}^{\alpha-2L}}\right\}\varepsilon, \quad \alpha < \xi \le L. \tag{14}$$

Strain Profiles and the Fragmentation Process

In this section, we illustrate important aspects of the behavior of the micromechanical model as it pertains to progressive fragmentation. Consider a long LE filament embedded in a bundle of HE filaments. As the bundle is extended, the strain in the LE filament and the neighboring HE filaments is initially uniform and equal to the applied strain ε. As the nominal breaking strain of the LE filament material is reached, a first isolated break occurs along the LE filament at the location of the most critical flaw. The strain is zero at the site of the break, recovering eventually to the applied value over some distance, the

Downloaded from http://trj.sagepub.com at US ARMY SOLDIER BIOCHEM COMM on May 8, 2008
© 2006 SAGE Publications. All rights reserved. Not for commercial use or unauthorized distribution.

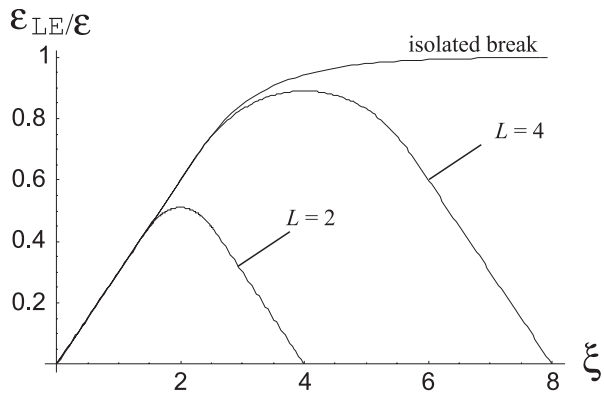

Figure 3 LE filament strains near an isolated break and for fragment of length $L = 2$ and $L = 4$. $Q = 0.3$ in all cases.

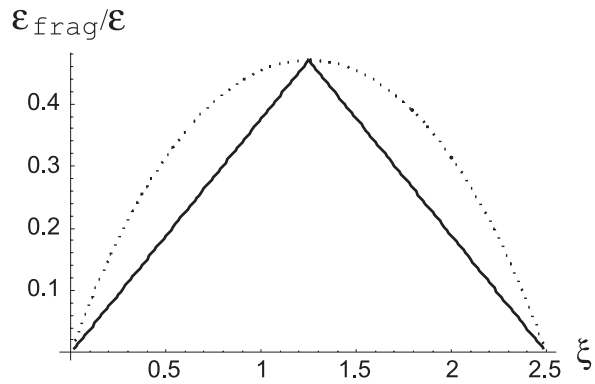

Figure 4 Fragment strain profile for limiting cases of no slip ($\alpha \to 0$), dotted line, and complete slippage ($\alpha \to L$), solid line, $L = 1.25$ for both cases. $Q = 0.848$ for no slip, and $Q = 0.376$ for complete slippage.

physical size of this recovery zone depending both on the slip region extent and the elastic properties of the LE filament and the filament/bundle interface. As the applied strain increases, additional breaks occur along the filament at other less critical flaws. As these subsequent breaks become closer together, the filament sections may be considered to be fragments. Here we use the term *fragment* to refer specifically to filament sections short enough such that the strain in the fragment never recovers fully to the applied value ε. The strain profile of a fragment is affected by the proximity of the two breaks at the fragment tips. Clearly, when the applied strain becomes significantly higher than the nominal LE filament breaking strain, the LE material must form fragments in order to lower the strain in the LE filament material to a survivable level. As bundle strain increases, the fragmentation process is progressive. Given that the largest strains in a fragment are concentrated toward the midpoint, fragments of length $2l$ will break yielding two fragments of approximate length l, each in turn breaking into two fragments of length $l/2$, and so on.

To illustrate the above points, the LE filament strains near an isolated break and the strain profiles for fragments of length $L = 2$ and $L = 4$ are exhibited in Figure 3, where $Q = 0.3$ in all cases. The solution for the isolated break case is obtained in the same way presented for the fragment case with the exception that, in lieu of the boundary condition at $\xi = L$, the positive exponential term in the solution for U_{II} is discarded in order that displacements in region II remain bounded at $\xi = \infty$. It can easily be shown that the LE filament strains for the isolated break case are given by $\varepsilon_{LE} = Q\xi\varepsilon$, $\xi \le \alpha$ (region I), where $Q = 1/(\alpha + 1)$; and $\varepsilon_{LE} = (1 - e^{\alpha-\xi}/(\alpha + 1))\varepsilon$, $\xi > \alpha$ (region II). For the isolated break, the strain is seen to recover to essentially the applied value for ξ greater than about five. For the fragments, the largest strains are seen concentrated near the midpoint, particularly so for the $L = 2$ case. The peak strain is 0.89ε for $L = 4$ and 0.51ε for $L = 2$. Therefore, neglecting statistical aspects, an $L = 2$ fragment may reasonably be expected to survive applied strains up to twice the nominal LE filament breaking strain for $Q = 0.3$.

The shape of the fragment strain profile is governed by the slip region extent, α. For large slip regions, $\alpha \to L$ (small Q), the profile becomes triangular, while for small slip regions, $\alpha \to 0$ (large Q), the profile is hump-shaped with a broader peak strain summit (Figure 4).

The effects of fragment length and Q on peak fragment strains (occurring at the fragment midpoint) are exhibited in Figure 5. Peak strains are seen to increase with increasing fragment length, depending strongly on fragment length for shorter fragments with half-lengths $L \le 4$. Peak strains are seen to increase with increasing Q. For large fragments, the peak strain approaches the applied strain, particularly for larger values of Q. For values of Q of 0.3 and greater, fragments half-lengths of $L = 4$ or greater attain peak strains close to the applied strain.

The dependence of peak strain on fragment length affects the fragmentation process in a fundamental way. In the early part of fragmentation, breaks are widely separated, and the strain in filament sections between the breaks is close to the applied strain. The initial phase of the process is therefore driven primarily by the distribution of flaws along the filament. As the breaks become closer together, such that the intervening fragments have half-lengths L of four or less (for Q values of 0.2 or greater), the peak strains

Downloaded from http://trj.sagepub.com at US ARMY SOLDIER BIOCHEM COMM on May 8, 2008
© 2006 SAGE Publications. All rights reserved. Not for commercial use or unauthorized distribution.

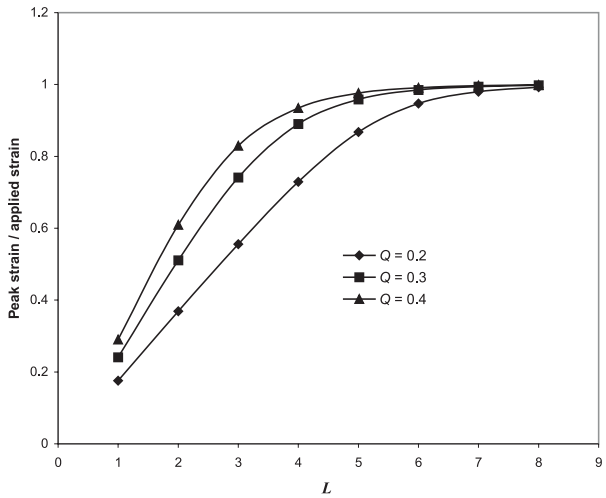

Figure 5 Peak fragment strain behavior with increasing *L*, various *Q*.

are strongly affected by fragment length, therefore, the longer fragments have much higher probabilities of fracturing at a given applied strain than shorter fragments. This later stage of fragmentation is driven by fragment size and the mechanics of the fragment interaction with the surrounding material. It should be noted that for very small Q values even fragments with large L values are slipping over most of their length and the peak strains remain strongly affected by fragment length at higher L values.

Behavior of Q and q_s during Extension of a Twisted Fibrous Structure

As a yarn or other twisted fibrous structure is extended, lateral compression in the body of the yarn increases with the increasing tension along the yarn axis. This feature of the interaction between tension and geometry is key to the self-locking behavior [4] of short fiber yarns. For a first-order approximation, consistent with the small strain analysis given by Hearle [3], we assume that the lateral compressive stress or pressure, p, acting on the fragment is proportional to the bundle axial strain, $p \propto \varepsilon$. Making the further assumption that Amontons' Law holds, the frictional shear stress at the slipping fragment surface may be written as $\tau_s = \mu p$, where μ is the coefficient of friction between the LE fragment and HE filament surfaces. Therefore, the slipping shear force per length, $q_s = \tau_s \pi d$, where d is the LE fragment diameter, is seen to be proportional to the applied strain, $q_s \propto \varepsilon$. Recalling the Q's definition, $Q = \dfrac{q_s}{\varepsilon\sqrt{kEA}}$, it is seen that the dependence of Q on ε is lost under these assumptions. Therefore, in a very crude, approximate way, we expect Q to remain constant with increasing strain. As such, the slip region extent along a fragment embedded in a twisted fibrous structure should remain fairly constant as the structure is extended. Similarly, properly constructed short fiber yarns are self-locking; they do not rupture by localized slipping apart of fibers as would happen if slip extents tended to grow with increasing yarn extension.

Practical twisted fibrous structures often deviate significantly from the restricted conditions that lead to a constant Q during extension. Synthetic filaments such as nylon and polyester have nonlinear load–extension behavior and twisted structures may in end-use undergo extensions that involve relatively large changes in geometry going from the initial to final deformed state. The actual behavior of Q in a given structure will depend on the combined effects of the constitutive behavior of the fibers, geometry changes of the structure, as well as the frictional behavior of the abutting fiber surfaces. While Q may be an increasing or decreasing function of increasing strain, we expect that q_s will ordinarily be a monotonically increasing function of strain, where the proportionality may be less than linear over the range of behavior of interest, i.e. $q_s \propto \varepsilon^m$, $0 < m < 1$.

Fracture of a Fragment under Increasing Applied Strain

In this section, we develop the statistical theory for fracture of a fragment under increasing bundle strain, where the strain profile along the fragment influences the probability of fracture. The widely used two-parameter Weibull distribution is adopted to model the failure strain of the LE filament material. The cumulative distribution function for failure of a filament of length $\bar{l}$, at a uniform strain $\bar{\varepsilon}$ is given by

$$F_{\bar{l}}(\bar{\varepsilon}) = 1 - \exp\left\{-(\bar{l}/\bar{l}_0)(\bar{\varepsilon}/\bar{\varepsilon}_{\bar{l}_0})^{\bar{\rho}}\right\}, \tag{15}$$

where $\bar{l}_0$ is a reference length (usually a test specimen gage length), $\bar{\varepsilon}_{\bar{l}_0}$ is the scale parameter, and $\bar{\rho}$ is the shape parameter. In the fragment, the strain profile is non-uniform, as discussed previously. Our interest is in the failure of the fragment at particular applied strains in the bundle. The cumulative distribution function for the applied strain associated with fracture of a fragment, length $2l$, may be written as

Downloaded from http://trj.sagepub.com at US ARMY SOLDIER BIOCHEM COMM on May 8, 2008
© 2006 SAGE Publications. All rights reserved. Not for commercial use or unauthorized distribution.

$$F_{\text{frag}}(\varepsilon) = 1 - \exp\left\{-\frac{2}{\bar{l}_0}\int_0^{l}\left(\frac{\varepsilon_{\text{frag}}(x,\varepsilon)}{\bar{\varepsilon}_{\bar{l}_0}}\right)^{\bar{\rho}} \mathrm{d}x\right\} \tag{16}$$

where the Weibull scale and shape parameters, $\bar{\varepsilon}_{\bar{l}_0}$ and, $\bar{\rho}$ are the same as in equation (15), and the fragment strain, regarded as a function of position, x, and the bundle applied strain, ε, is symmetric with respect to the specimen midpoint. For the development of equation (16), the reader may refer to Phoenix and Beyerlein [6, pp. 585–586], where the development of a similar expression is outlined. In dimensionless quantities, the distribution becomes

$$F_{\text{frag}}(\varepsilon) = 1 - \exp\left\{-\frac{2}{\bar{L}_0}\int_0^{L}\left(\frac{\varepsilon_{\text{frag}}(\xi,\varepsilon)}{\bar{\varepsilon}_{\bar{L}_0}}\right)^{\bar{\rho}} \mathrm{d}\xi\right\} \tag{17}$$

where $\bar{L}_0$ is the nondimensional reference length, $\bar{l}_0 = \sqrt{EA/k}\bar{L}_0$, and ξ and L are the dimensionless position coordinate and half fragment length introduced earlier.

To relate the fragment fracture probability to the outcome of fragmentation experiments, we use the concept of a characteristic fragment length, defined here as the half-length of a fragment having a probability of fracture of 0.5 at a particular applied strain. A similarly defined characteristic fragment length was introduced as a measure of mean fragment length by Handge *et al.* in work on scaling relationships in the fragmentation of polymeric coatings [7]. Denoting the characteristic length by L_c, putting the fragment strain profiles in equations (13) and (14) into equation (17) and setting the probability equal to 0.5, we obtain,

$$\exp\left\{-\frac{2Q^{\bar{\rho}}}{\bar{L}_0}\int_0^{\alpha}\left(\xi\frac{\varepsilon}{\bar{\varepsilon}_{\bar{L}_0}}\right)^{\bar{\rho}} \mathrm{d}\xi - \frac{2}{\bar{L}_0}\int_{\alpha}^{L_c}\left(\left[1 - \frac{\mathrm{e}^{-\xi} + \mathrm{e}^{\xi - 2L_c}}{(1+\alpha)\mathrm{e}^{-\alpha} + (1-\alpha)\mathrm{e}^{\alpha - 2L_c}}\right]\frac{\varepsilon}{\varepsilon_{\bar{L}_0}}\right)^{\bar{\rho}} \mathrm{d}\xi\right\} = 0.5 \tag{18}$$

where Q is given by equation (9) with $L = L_c$. Equation (18) may be used to calculate values of α and Q for given values of L_c, applied strain ε, and the Weibull shape and scale parameters. As such, where the characteristic length can be estimated through appropriate experiments, equation (18) provides a description of the force interactions and interfacial behavior of the fragment and neighboring fibrous material.

Experiments

The two-component strand studied here is a model structure. Individual cotton and polyester yarns serve as surrogates for LE and HE fibers, respectively. Using yarns as surrogates for fibers, inspired by the pioneering experiments of Monego and Backer on model blended strands [8, 9], allows for fragments to be to manipulated and measured with ease. The strand specimens, with a single LE component embedded in a "matrix" of HE components are analogous to the single filament composite (SFC) specimens [10] used to study interfacial shear strength in fiber composites.

Specimens were prepared by helically wrapping 24 polyester sewing threads (HE component) around a straight central cotton sewing thread (LE component). Both the HE and LE threads were 35 tex. The cotton thread was kept straight by hanging a small weight from the end while the polyester threads were twisted about the central thread, maintaining a relatively consistent number of turns per length. The number of turns per length averaged 246 m^{-1} and specimen diameter averaged 1.08 mm. Nominal helix angle of the polyester threads was 40° from the strand centerline. A cardboard "frame" was used to hold the specimen in place for testing.

An Instron testing machine was used to apply increasing tension on the specimen under displacement control (25.4 mm/min, 1.0 inch/min). The gage length was 15.24 cm. Tests were performed over a range of maximum strain levels. Initial thread failure of the LE component was observed by studying the load–strain curves, which reveal the point where load drop occurred. These data were noted and used to determine shape and scale factors for the LE thread. Successive breaks in the LE thread were heard and could also be observed in the load–strain curve.

Specimens were examined by carefully removing the HE thread and recording the number and length of LE thread fragments. The length of the longest fragment (about to break) and the most recently broken fragment were recorded for use in the statistical model. The most recent break was determined through "forensic" examination of the fragment tips. As the fragments are strained, the ends are drawn and pulled by the polyester wrap; therefore, fragments generated early in the test had tips that appeared frayed. Fragments generated toward the end of the test had ends with a clean, almost cut appearance. In many cases, the most recently broken fragments appeared intact. The most recently broken fragment was determined by selecting the pair which either appeared unbroken or that had the "cleanest" cut.

The objective was to test a sufficient number of specimens to obtain approximately 100 fragments per strain level. Tests were performed at strain levels of 8, 10, 12, 15, and 18%, which produced on average six, 10, 11, 15, and 17 fragments per specimen, respectively. Therefore, it was necessary to test more specimens at the lower strain levels to generate an adequate number of fragments.

Downloaded from http://trj.sagepub.com at US ARMY SOLDIER BIOCHEM COMM on May 8, 2008
© 2006 SAGE Publications. All rights reserved. Not for commercial use or unauthorized distribution.

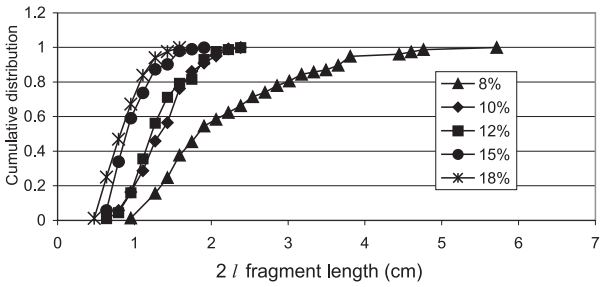

Figure 6 Experimental cumulative fragment length distributions.

Analysis of Fragment Lengths

The cumulative distribution of fragment lengths, $2l$, for specimen strains of 8, 10, 12, 15, and 18% are exhibited in Figure 6. It can be seen that for specimen strains of 10% and greater, the shape of the fragment length distributions is quite similar, with the overall distribution being shifted toward shorter fragments with increasing strain levels. The shape of the distribution is quite different for the 8% series, however. At 8% strain, the specimen is still experiencing transition from early fragmentation, in which the process is dominated by the presence of flaws rather than the mechanics of the fragment interaction with the surrounding medium. As will be discussed later in this section, the 8%experiments are not useful for the recovery of information about the fragment interaction, because fragment length is not strongly driving the fragmentation process at this stage.

The characteristic fragment lengths were estimated in the following way. As previously mentioned, the specimen was disassembled, and the cotton thread was carefully extracted. The most recent break was identified by its condition, as described in the preceding section. The lengths of each fragment in order as they occurred in the specimen was recorded, and the length of the most recently broken fragment was recorded as the sum of the fragment lengths on either side of the most recent break. The length of the longest surviving fragment in each specimen was also recorded. After the series of tests at a given strain level was complete, the characteristic fragment length, $2l_c$, was estimated as the average of the lengths of the most recently broken fragment and longest surviving fragment in each specimen. This procedure is similar to the calculation of the ballistic limit velocity, V_{50}, the velocity at which a projectile has a 50% probability of penetrating an armor panel, from the average of a set of the highest velocity non-penetrating and lowest velocity penetrating impacts.

The non-dimensional characteristic lengths, L_c, are calculated from the dimensional lengths using $L_c = \sqrt{k/EA}l_c$, from the length scaling of equation (2a). The value of k, taken to be 8.39 MPa, was estimated from measurements of the cotton thread shear modulus using a torsion pendulum set-up. The axial stiffness, EA, was determined to be 144.56 N from linear fits to the load–strain curves obtained from extension testing of cotton thread specimens.

The value of the non-dimensional shear force, Q, acting on the cotton fragments at the various strain levels is calculated from the L_c values using equation (18) by varying the slip region extent, α, until equation (18) is satisfied. The values of the shape and scale parameters, $\bar{\rho} = 9.652$ and $\bar{\varepsilon}_{\bar{l}_0} = 3.676\%$, were determined from the strains at the first break of the cotton thread in the entire series of tests. The dimensional slip shear force, q_s, is calculated using the definition of Q as $q_s = Q\varepsilon\sqrt{kEA}$. The values of the various parameters calculated from the analysis of the fragment lengths are tabulated in Table 1. The average fragment length, $< 2l >$, is also listed for comparison.

The Q values are seen to be generally declining slightly, and the q_s values generally increasing, with considerable scatter, for strain levels of 10 through 18%. For the 8% strain level, the computed Q value is much lower than the 10% value, due to the much larger fragment lengths seen in the

Table 1 Parameter values determined from fragmentation experiments.

Strain level:	8%	10%	12%	15%	18%
$< 2l >$ (cm)	2.33	1.43	1.37	1.04	0.927
$2l_c$ (cm]	3.68 (0.923)*	2.13 (0.288)	2.11 (0.237)	1.59 (0.249)	1.55 (0.437)
L_c	4.43	2.57	2.55	1.91	1.87
α	4.03	2.11	2.23	1.60	1.62
Q	0.150	0.224	0.186	0.206	0.174
q_s (N/m)	417	781	775	1076	1090

* Standard deviation of the mean of most recently broken and largest fragment lengths in parentheses.

Downloaded from http://trj.sagepub.com at US ARMY SOLDIER BIOCHEM COMM on May 8, 2008
© 2006 SAGE Publications. All rights reserved. Not for commercial use or unauthorized distribution.

8% test series. The low value of Q and q_s from the 8% fragment data is physically unreasonable based on our general understanding of how these properties should behave and is inconsistent with the trend in q_s values predicted from strand geometry in the section to follow. As mentioned above, the fragment distribution clearly demonstrates a different regime of behavior is at work at the 8% strain level. A much wider distribution of fragment lengths is present at 8%, thereby making the determination of the critical fragment length imprecise.

Modeling Frictional Shear Force from Deformed Strand Geometry

The analysis of fragment lengths from the experimental specimens has provided a means to quantify the values of the slip frictional shear force on the fragment, and the slip region extent along the fragment. To check whether these values are physically reasonable, an analysis is presented in this section to estimate the likely value of the slip frictional shear force based on the deformation of the helically wound strand structure. Here we assume the slip frictional shear force per length q_s acting on the cotton fragment is proportional to the lateral pressure in the center of the specimen (Amontons' Law). The approach for estimating the lateral pressure in the experimental strand is described in the following.

As described previously, the strands are made by helically wrapping 24 polyester threads, in four bundles of six, around the center cotton thread, such that all polyester threads have approximately the same helix angle. The arc length along the centerline of polyester threads lying toward the center of the strand will, therefore, be less than the arc length along threads lying on the surface in a given short segment of the strand (over long distances the threads change position in the strand to equalize arc length differences). It is likely that the inner polyester threads will be locally buckled as a result of arc length differences between inner and surface layers of the threads. As the strand is extended, the helical path of each polyester thread increases in arc length and each thread develops tension in accordance with the increased thread strain. Transverse force equilibrium of each curved thread under tension requires a radially outward directed distributed force acting at the centerline of the thread (Figure 7) arising from contact with neighboring threads. The equal and opposite distributed radial force acting on the rest of the strand due to the thread acts to compress the strand and contributes to the development of lateral pressure, as shown schematically in Figure 7. It is assumed here that, due to the initially buckled condition of subsurface polyester threads and their resulting low tension, only the outer surface layer of threads significantly contributes to the development of lateral pressure, and the contribution of inner layers may be neglected.

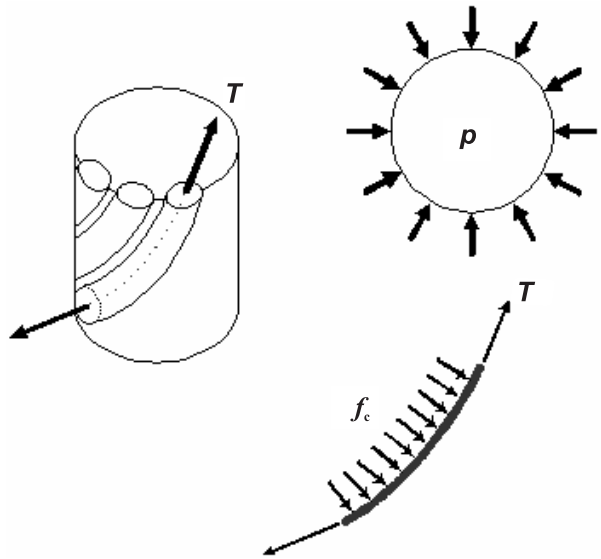

Figure 7 Development of lateral pressure in strand due to outer layer thread tension.

Inspection of the experimental strands reveals that there are an average of ten threads in the outer layer, $n_{OL} = 10$, and these threads are substantially not in contact circumferentially (Figure 7). Therefore, by smearing out the radially inward helical contact line loads due to the ten outer layer threads over the surface area of the strand, we obtain the effective lateral pressure in the strand center.

The contact line load, f_c, may be obtained from transverse force equilibrium of an element of the thread as

$$f_c = \frac{T(\varepsilon_{OL})}{\rho}, \tag{19}$$

where $T(\varepsilon_{OL})$ is the thread tension as a function of the strain in the outer layer thread, and ρ is the radius of curvature of the thread centerline in the deformed geometry. From geometry, ε_{OL} is obtained as

$$\varepsilon_{OL} = \left\{ \frac{(1+\varepsilon)^2 + 4\pi^2 r^2 t^2}{1 + 4\pi^2 r_i^2 t^2} \right\}^{1/2} - 1, \tag{20}$$

where ε is the specimen strain, r is the current strand radius, r_i is the initial strand radius, and t is the number of turns/m that the helix takes as made. In practice, while measurements were made of initial and final strand diameters in the experiments, a more consistent means of modeling the final strand radius was obtained by assuming constant volume deformation of the strand with some fixed consolidation,

Downloaded from http://trj.sagepub.com at US ARMY SOLDIER BIOCHEM COMM on May 8, 2008
© 2006 SAGE Publications. All rights reserved. Not for commercial use or unauthorized distribution.

$$r \cong \frac{c}{\sqrt{1+\varepsilon}} r_i, \tag{21}$$

where c was determined to be 0.97 for good agreement with measurements. In the calculations done here, $T(\varepsilon_{OL})$ is determined by fitting a cubic polynomial to the polyester thread load–strain curve for strains up to 10%, and evaluating the cubic at the outer layer thread strain determined using equation (20). From geometry, the radius of curvature is found to be

$$\rho = r + \frac{(1+\varepsilon)^2}{4\pi^2 r t^2}. \tag{22}$$

Combining (22) and (19) and rearranging, f_c may be written as

$$f_c = T(\varepsilon_{OL}) \frac{4\pi^2 r t^2}{(1+\varepsilon)^2 + 4\pi^2 r^2 t^2} \tag{23}$$

It should be noted that equation (23) represents the contact line load as a force per unit length of the deformed (strained) contact line. Leech [11] derives a similar expression for a contact force per unit original length of a helical rope component using the principle of virtual work. Conversion of contact force in Leech [11] to a per-unit deformed length basis, multiplying by a factor of $1/(1 + \varepsilon_{OL})$, yields an expression equivalent to equation (23).

For a helix angle of β with respect to the strand axis, the total load per specimen length due to the surface layer contact line loads is $f_c n_{OL}/\cos\beta$, where from geometry of the helix, $\cos\beta = (1 + \varepsilon)/[(1 + \varepsilon)^2 + 4\pi^2 r^2 t^2]^{1/2}$. The lateral pressure, p, calculated as the total load per specimen surface area, may be seen to be $f_c n_{OL}/(2\pi r \cos\beta)$. Using equation (23), the lateral pressure is written as

$$p = T(\varepsilon_{OL}) n_{OL} \frac{4\pi^2 r t^2}{\left[(1+\varepsilon)^2 + 4\pi^2 r^2 t^2\right]^{1/2} (1+\varepsilon)}. \tag{24}$$

The slip frictional shear force, using Amontons' Law, is obtained as, $\hat{q}_s = \mu\pi d p$, where πd is the cotton thread circumference, and μ is the coefficient of friction. However, in its present form $\hat{q}_s$ represents a shear force per unit extended length of the strand. The shear force per length is defined in the micro-mechanical model as a force per length along the x-axis, where the x-coordinate represents position in the original (unstrained) geometry of the strand. Therefore, for consistency with the shear force values obtained through the micromechanical model from the fragmentation experiments, the shear force per unstrained strand length is obtained as

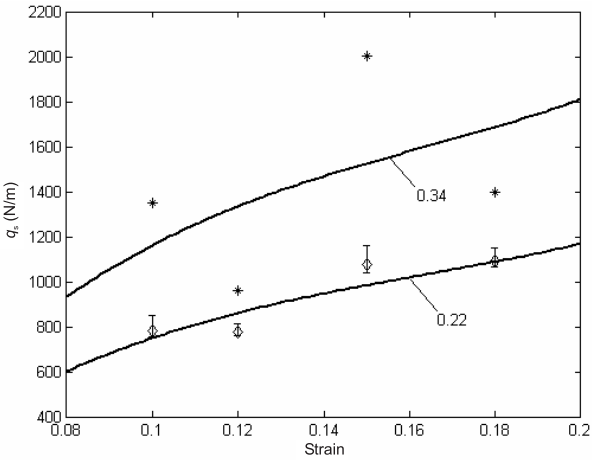

Figure 8 Frictional shear force per length, q_s, in experimental strands. Behavior calculated from deformed strand geometry is shown with solid lines, coefficient of friction is as indicated. Diamond markers indicate q_s derived from fragment lengths for the estimated value of $k = 8.39$ MPa. Error bars indicate range of q_s based on $k = 4.20$ MPa, upper bar, and complete slippage, lower bar. Asterix markers indicate q_s for $k_{min} = 2.18$ MPa.

$$q_s = (1+\varepsilon)\mu\pi d p, \tag{25}$$

where p is given by equation (24).

The frictional shear force, calculated using equation (25), is exhibited over a range of strain levels in Figure 8, alongside the values determined through the fragment length data (diamond markers; error bars will be discussed in the following section). In these calculations, average values for the helix twist, $t = 246$ turns/m, and the specimen initial radius, $r_i = 0.54$ mm, were used, and the frictional coefficient, μ, has been taken to be 0.22 for a best fit to the experimentally derived values. For strand strains ranging from 8 to 20%, the outer layer thread strains were found to range from 2.3 to 8.2%, thread tension ranged from 1.5 to 3.3 N, and lateral pressure ranged from 4.4 to 8.9 MPa. Given that pressure varied by only a factor of two over the range of extension, the assumption that the coefficient of friction is constant during strand extension is a good approximation.

Discussion

We have developed a failure distribution for a LE fragment embedded in a medium of HE filaments based on a micro-

Downloaded from http://trj.sagepub.com at US ARMY SOLDIER BIOCHEM COMM on May 8, 2008
© 2006 SAGE Publications. All rights reserved. Not for commercial use or unauthorized distribution.

mechanical model and used this distribution in conjunction with a critical length concept to interpret fragmentation experiments and reveal key information about the fragment's force interaction with the surrounding material. The reasonable agreement between the shear force per length, q_s, values calculated from the fragmentation data and the trend in q_s exhibited by the analysis of the deformed geometry of the strand suggests that the fragmentation-derived values are indeed plausible. As discussed previously, the values are obtained based on satisfaction of equation (18), where the fragment length L_c is regarded as a known quantity, scaled from the experimental fragment lengths using the values of the constitutive parameters EA and k. As such, the certainty with which these key constitutive parameters are known plays a central role in the confidence we place in our estimates of the force interaction parameters α, Q and q_s. In the following, we examine how the possible ranges of values of the constitutive parameters affect the force interaction behavior developed from the fragmentation data, and thereby establish secure bounds on the force interactions occurring in the experiments.

While EA is well known through direct measurements of the cotton thread specimen load–-displacement behavior, the value used for k is regarded as only a rough estimate, where we have assumed that k may be approximated by the shear modulus of the cotton thread in torsion. Therefore, the effects of varying the value of k on the interpretation of the fragment length data using the critical length calculation (equation (18)) need to be examined critically.

We note that, due to the non-dimensionalization scheme, $L \propto k^{1/2}$. Decreases in k therefore make the fragment appear shorter in the framework of the model. Since shorter fragments develop less strain relative to the applied strain in the bundle, where both a short fragment and a long fragment are under conditions such that their cumulative failure probabilities are 0.5 (i.e., they are *critical length*), the short fragment will exhibit a shorter slip extent relative to its length, and consequently, a higher value of Q. Put another way, to satisfy the critical length equation for a given physical value of l_c and bundle strain from the experiment, with a decreased value of k, L_c will be smaller, and the value of α that satisfies equation (18) will become much smaller. At some point, for decreasing k a threshold is reached where equation (18) can no longer be satisfied, even for $\alpha = 0$. This threshold defines the minimum value of k consistent with the fragmentation data. For values of k less than the minimum, the fragments are too short in the framework of the model to produce sufficiently large strain amplitudes for fracture.

For increasing k, the opposite situation holds. Fragment lengths appear longer to the model, and slip extents become increasingly large relative to the fragment length in order to satisfy the critical length equation. A simple limiting case can be developed, where the fragment slips along its entire length, and the parameter k no longer enters the picture because there is no elastic interaction with the surrounding material. For a slipping fragment, the strain in the region $0 \le x \le l$ is simply $\varepsilon_{frag} = q_s x/EA$. Using this strain profile in the dimensional version of the fragment failure distribution, equation (16), completing the integration, and setting the probability equal to 0.5 for the critical length results in

$$\exp\left\{\frac{-2}{\bar{l}_0}\left(\frac{q_s}{EA\bar{\varepsilon}_{\bar{l}_0}}\right)^{\bar{\rho}}\frac{l_c^{\bar{\rho}+1}}{\bar{\rho}+1}\right\} = 0.5. \tag{26}$$

Using equation (26) to evaluate q_s for the complete slippage case from the characteristic fragment length data gives q_s = 753, 759, 1041, and 1067 N/m for the 10, 12, 15 and 18% strain levels, respectively.

In Table 2, the parameters are tabulated for a range of k values, one being the limiting case of the minimum k for which solutions could be obtained for each fragmentation test series (10 through 18%). For the non-minimum cases, k values of 0.5, twice and 10 times the estimated value of 8.39 MPa were chosen. It can be seen that for larger values

Table 2 Parameter values for various k.

	L_c	α	Q	q_s (N/m])
k_{min} = 2.18 MPa				
10%	1.31	0.113	0.761	1351
12%	1.3	0.588	0.45	958
15%	0.975	0.000	0.751	2001
18%	0.955	0.376	0.436	1395
k = 4.20 MPa				
10%	1.81	1.16	0.345	848
12%	1.8	1.33	0.275	814
15%	1.35	0.885	0.315	1162
18%	1.32	0.963	0.259	1148
k = 16.78 MPa				
10%	3.63	3.3	0.155	761
12%	3.6	3.37	0.129	764
15%	2.7	2.48	0.142	1051
18%	2.65	2.47	0.121	1073
k = 83.9 MPa				
10%	8.11	7.96	0.0684	753
12%	8.05	7.94	0.0575	760
15%	6.05	5.95	0.0631	1042
18%	5.92	5.84	0.0538	1067

Downloaded from http://trj.sagepub.com at US ARMY SOLDIER BIOCHEM COMM on May 8, 2008
© 2006 SAGE Publications. All rights reserved. Not for commercial use or unauthorized distribution.

of k, the slip region extent α increases relative to L_c – the fragments are slipping over a greater fraction of their length. Values of q_s for $k = 83.9$ MPa are essentially the same as for the complete slippage case.

The range of possible q_s values derived from the fragmentation data for $k > 4.20$ MPa, where complete slip represents $k \to \infty$, are plotted in Figure 8 as error bars on the data for the estimated value of 8.39 MPa (upper error bar indicates q_s for $k = 4.20$ MPa, lower error bar indicates q_s for $k \to \infty$). It can be seen that for this range of k, 4.20 MPa $\leq k < \infty$, the q_s values cluster together and correspond well with the projections based on the strand geometry with $\mu = 0.22$. The values of q_s for the theoretical minimum value of k, exhibited in Figure 8 (asterix markers), are seen to be significantly scattered, rather than following a smooth trend, and generally much higher than the values for larger k. The strand geometry projection for $\mu = 0.34$ is shown for comparison with the minimum k behavior. For $k = k_{min}$, q_s is particularly high for the 15% nominal strain series, because the slip region extent is zero in that case, leading to the highest possible value of q_s. The large scatter in q_s for k_{min} seems unlikely compared with the much smaller scatter exhibited when k takes on larger values, particularly considering that each data point is calculated from a mean of many fragment lengths. Therefore, while k could theoretically have a value as small as 2.18 MPa, it appears that k most likely has a value of about 4 MPa or greater. As such, considering the results for α, the LE fragments are interacting with the surrounding HE threads primarily through frictional slip, where 70% or more of the fragment is slipping. The most likely range of q_s is considered to be the range of values bounded by the $k = 4.20$ MPa results at the high end, and the complete slippage results at the low end.

It is interesting to look at the fragment strain profiles corresponding to the solutions for different k. In Figure 9, strain profiles for the critical length fragment from the 10% strain experiments are plotted for complete slippage, $k = 8.39$ MPa, 4.20 MPa, and the minimum value of 2.18 MPa. The triangular profile for complete slippage has the highest peak strain. In comparison, the $k = 8.39$ MPa results show a slightly lower peak strain with slightly steeper linear profiles away from the fragment middle. These differences intensify for the $k = 4.20$ MPa results, and particularly so for $k = 2.18$ MPa. Each of theses strain profiles represents a condition under which half of such fragments would be expected to have fractured at a specimen nominal strain of 10%.

It has been shown, through this discussion, that analysis of fragment lengths from fragmentation experiments, similar to those here, can provide some insight into the force interactions between the fragment and the fibrous structure. Clearly, the precision with which this information can be interpreted relies heavily on the precision with which certain constitutive parameters can be determined. We have shown that there is a theoretical minimum value for k, as well as another limiting case of complete slip, and these bounding cases define a range of values for the frictional slip shear force per length that is possible based on the experimental fragment length results. Based on comparison of the fragmentation-derived results with a projection of the shear force based on strand geometry, we have asserted that the most likely values for the parameter k are somewhat higher than the theoretical minimum and closer to the estimate made by torsion pendulum measurements.

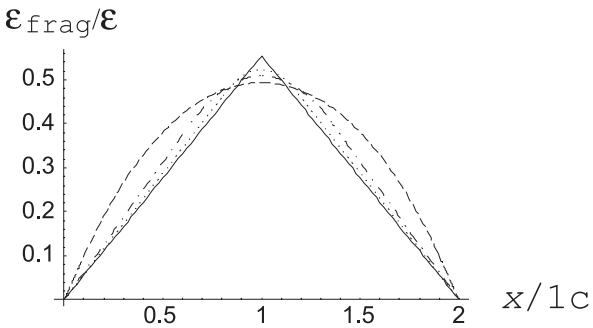

Figure 9 Possible fragment strain profiles for critical length fragment from 10% strain series. Solid line, complete slippage; dotted line, $k = 8.39$ MPa; dot-dashed line, $k = 4.20$ MPa; dashed line, $k_{min} = 2.18$ MPa.

Conclusions

We have investigated the interaction between a low elongation-to-break (LE) fragment and the surrounding fibrous medium during extension and progressive fragmentation of a model two-component fibrous structure using a simple micromechanical model. The model fibrous structure, representing a blended yarn or cord, was realized in experimental specimens by helically wrapping a number of high elongation-to-break (HE) components around a straight central LE component; polyester and cotton sewing threads served as surrogates for HE and LE fibers. The concept of a characteristic fragment length, involving the failure statistics of a fragment as influenced by the interaction forces between the fragment and the fibrous medium, was used to interpret the fragmentation experiments and calibrate a dimensionless parameter in the micromechanical model. The calibrated model was shown to provide insight into the magnitude of the frictional slip shear force and extent of the slipping region along the fragment. Bounds were established on the range of the frictional slip shear force acting on the fragments in

Downloaded from http://trj.sagepub.com at US ARMY SOLDIER BIOCHEM COMM on May 8, 2008
© 2006 SAGE Publications. All rights reserved. Not for commercial use or unauthorized distribution.

the experiments based on limiting cases. The values of the slip shear force derived from the fragment data were in agreement with projections based on analysis of the deformed geometry of the helically wound strands and Amontons' Law. Results showed that the LE fragments interacted primarily through slip with the HE wrapping, with the slip occurring along 70% or more of the fragment's length.

Literature Cited

1. Achenbach, J.D., and Zhu, H., Effect of Interfacial Zone on Mechanical Behavior and Failure of Fiber -Reinforced Composites, *J. Mech. Phys. Solids* **37**, 381–393 (1981).
2. Chawla, K.K., "Composite Materials: Science and Engineering," Springer-Verlag, New York, 1987.
3. Hearle, J.W.S., Grosberg, P., and Backer, S., "Structural Mechanics of Fibers, Yarns, and Fabrics," Wiley-Interscience, New York, 1969.
4. Hearle, J.W.S., Mechanics of Yarns and Nonwoven Fabrics, in "Textile Structural Composites," T.W. Chou and F.K. Ko, Eds, Elsevier, Amsterdam, 1989.
5. Godfrey, T.A., and Rossettos, J.N., A Constitutive Model for Blended Yarn Extension with Fragmented Low-Elongation Fibers, *Textile Res. J.* **71**(10), 845–854 (2001).
6. Phoenix, S.L., and Beyerlein, I.J., Statistical Strength Theory for Fibrous Composite Materials, in "Comprehensive Composite Materials," Vol. 1, A Kelly and C. Zweben, Editors-in-chief, T.W. Chou, Volume 1 editor, New York: Pergamon, 2000, pp. 559–639.
7. Handge, U.A., Sokolov, I.M., and Blumen, A., Universal Scaling and Nonlinearity in Surface Layer Fragmentation, *Phys. Rev. E* **61**(3), 3216–3219 (2000).
8. Monego, C., "The Mechanics of Rupture of Cotton-Dacron Yarns," Masters Thesis, M.I.T., Cambridge, MA, 1963.
9. Monego, C.J., and Backer, S., Tensile Rupture of Blended Yarns, *Textile Res. J.* **38**, 762–766 (1968).
10. Drzal, L.T., Adhesion of Graphite Fibers to Epoxy Matrices: 1. The Role pf Fiber Surface Treatment, *J. Adhesion* **16**, 1–30 (1982).
11. Leech, C.M., The Modelling of Friction in Polymer Fibre Ropes, *Intl. J. Mech. Sci.* **44**, 621–643 (2002).

Downloaded from http://trj.sagepub.com at US ARMY SOLDIER BIOCHEM COMM on May 8, 2008
© 2006 SAGE Publications. All rights reserved. Not for commercial use or unauthorized distribution.